minerals

MDPI

Article

Properties of Sulfur Particles Formed in Biodesulfurization of Biogas

Annemerel R. Mol [1,2], Renata D. van der Weijden [1,3,*], Johannes B. M. Klok [1,2,3] and Cees J. N. Buisman [1,3]

1 Environmental Technology, Wageningen University & Research, P.O. Box 17, 6700 AA Wageningen, The Netherlands; annemerel.mol@wur.nl (A.R.M.); jan.klok@wetsus.nl (J.B.M.K.); cees.buisman@wur.nl (C.J.N.B.)
2 Paqell B.V., Reactorweg 301, 3542 AD Utrecht, The Netherlands
3 Wetsus, European Centre of Excellence for Sustainable Water Technology, P.O. Box 1113, 8900 CC Leeuwarden, The Netherlands
* Correspondence: renata.vanderweijden@wur.nl; Tel.: +31-317-483851

Received: 31 March 2020; Accepted: 3 May 2020; Published: 11 May 2020

Abstract: In the biodesulfurization (BD) process under halo-alkaline conditions, toxic hydrogen sulfide is oxidized to elemental sulfur by a mixed culture of sulfide oxidizing bacteria to clean biogas. The resulting sulfur is recovered by gravitational settling and can be used as raw material in various industries. However, if the sulfur particles do not settle, it will lead to operational difficulties. In this study, we investigated the properties of sulfur formed in five industrial BD facilities. Sulfur particles from all samples showed large differences in terms of shape, size, and settleability. Both single crystals (often bipyramidal) and aggregates thereof were observed with light and scanning electron microscopy. The small, non-settled particles account for at least 13.6% of the total number of particles and consists of small individual particles with a median of 0.3 µm. This is undesirable, because those particles cannot be removed from the BD facility by gravitational settling and lead to operational interruption. The particles with good settling properties are aggregates (5–20 µm) or large single crystals (20 µm). We provide hypotheses as to how the differences in sulfur particle properties might have occurred. These findings provide a basis for understanding the relation between sulfur particle properties and formation mechanisms.

Keywords: crystallization; full-scale desulfurization; particle size analysis; settleability; sulfur

1. Introduction

Biogas, natural gas, and other gases originating from anaerobic degradation of organic matter usually contain corrosive and toxic hydrogen sulfide (H_2S) [1–3]. By removing H_2S with desulfurization technologies before gas combustion, harmful effects (through sulfur dioxide formation) on process equipment and the environment are prevented [4,5]. Biodesulfurization (BD) of gas under halo-alkaline conditions is an attractive process, because it (i) utilizes naturally occurring bacteria instead of chelating chemicals to catalyze sulfide oxidation, (ii) operates at ambient pressure and temperature, (iii) has a high H_2S removal efficiency, (iv) produces re-usable biological sulfur, and (v) does not require stabilizers and solvents for sulfur in the process solution [6,7]. In the process (Figure 1), H_2S is removed from the gas stream by absorption into a mildly alkaline buffered process solution (pH 8–10), where it dissociates into bisulfide (HS^-; Equation (1)). In the subsequent process step, a mixed culture of halo-alkaline sulfide oxidizing bacteria (HA-SOB) oxidizes bisulfide to elemental sulfur (S^0) in a micro-aerophilic bioreactor (Equation (2)).

$$H_2S\ (g) \rightleftarrows H_2S\ (l) \rightleftarrows HS^- + H^+ \quad (1)$$

$$HS^- + H^+ + \frac{1}{2}O_2 \rightarrow S^0 + H_2O \quad (2)$$

In addition to the formation of solid elemental sulfur (hereafter referred to as "sulfur"), other sulfur species can be formed as by-products, such as sulfate (SO_4^{2-}) and thiosulfate ($S_2O_3^{2-}$). These soluble by-products need to be removed via an effluent stream. Hence, the formation of sulfur is preferred because contrary to the soluble by-products, it is a solid and can be separated from the process by sedimentation in, for example, a settler or decanter centrifuge. In addition, the separated sulfur has potential value as it can be reused in various industries as a raw material, as substrate for autrotrophic denitrification and metal bioleaching, and as fertilizer or fungicide in agriculture [8–15].

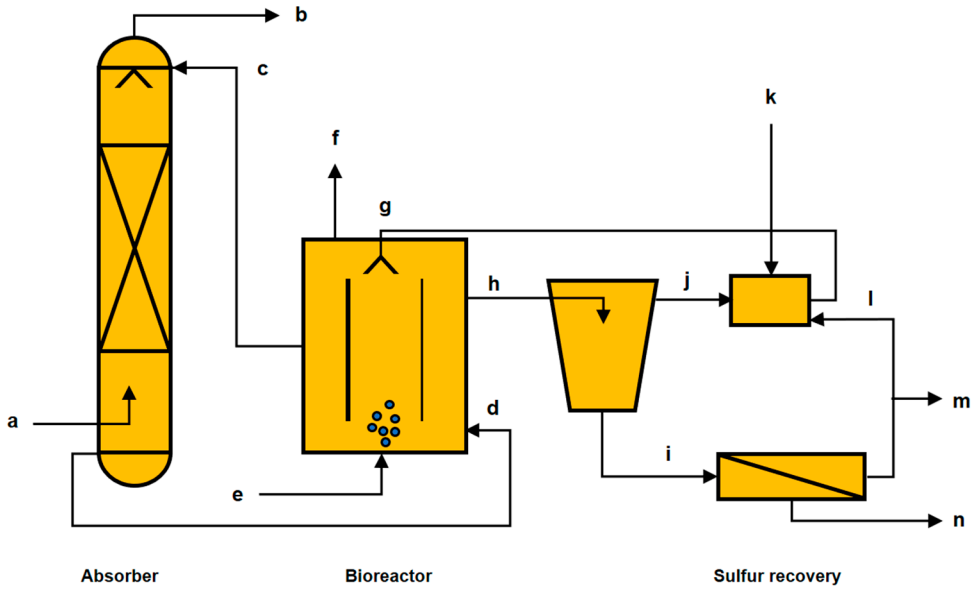

Figure 1. Flow scheme of the biotechnological process for gas desulfurization (adapted from [16]). (**a**) H_2S-rich gas; (**b**) H_2S-free gas; (**c**) H_2S-free solution; (**d**) H_2S-rich solution; (**e**) Air; (**f**) Air vent; (**g**) Make-up stream and recycled liquid fraction; (**h**) Sulfur rich solution; (**i**) Thickened sulfur stream from bottom of the settler; (**j**) Liquid fraction from top of the settler; (**k**) Make-up stream: nutrients, water and NaOH; (**l**) Residual liquid stream from sulfur separation; (**m**) Effluent stream; (**n**) Recovered sulfur.

For over 30 years, the BD process under halo-alkaline conditions has been implemented on an industrial scale and more than 270 full-scale installations have been realized [17,18]. Although the optimization of sulfur formation has been studied extensively [7,19–23], specific properties of the formed sulfur particles, such as size, morphology, and settleability remain an important subject of interest. In a variety of full-scale facilities (H_2S loads ranging from 50 kg sulfur day^{-1} up to 15 ton sulfur day^{-1}) operators and process engineers have observed different and fluctuating settleability of sulfur particles [24].

Formation of large sulfur particles is expected to result in well-settleable sulfur and adequate sulfur removal (Figure 2). Correspondingly, it is assumed that poor settleability is caused by the formation of small sulfur particles. When the formed sulfur particles are small, they do not settle and thus cannot be removed from the reactor solution. Especially if no decanter centrifuge is present in the process (often an economic consideration), removal of the sulfur is only achieved by a thickened effluent stream from the bottom of the settler. The liquid fraction from the top of the settler is separated and recirculated to the bioreactor. The thickened stream at the bottom of the settler is less concentrated if the sulfur does not settle, in which case a larger total effluent stream is needed to remove all elemental sulfur. The lost process liquid needs to be compensated for with NaOH and make-up water to maintain a suitable volume, conductivity, and buffer capacity. In addition, when poor sulfur settling occurs, the sulfur concentration increases in the reactor liquid and process operation is interrupted

by, for example, the clogging of process equipment. Moreover, small particles have a high surface to volume ratio and together with high sulfur concentration this leads to a high total surface area. A high total surface area is unwanted as (i) it is more prone to side reactions such as oxidation to SO_4^{2-} and (ii) it enhances foaming tendency, e.g., by enhancing the stabilization of gas bubbles [25]. Foaming may also cause operational interruption. All the aforementioned effects of small sulfur particle production lead to economic losses in the process.

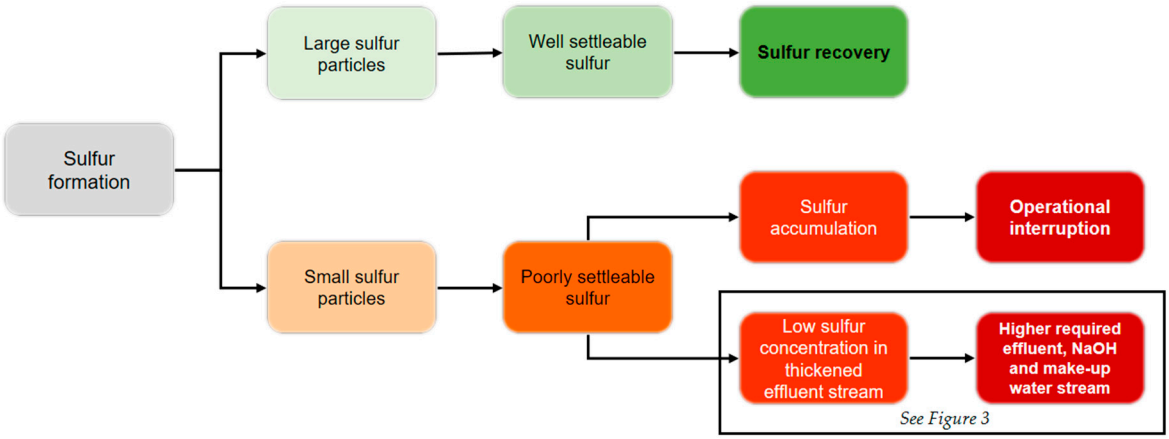

Figure 2. Effects of size of sulfur particles on operation of biodesulfurization (BD) process under halo-alkaline conditions.

From the process a continuous effluent stream is discharged, removing formed sulfur to prevent its accumulation. Sulfur accumulation leads to operational interruptions mentioned earlier. In addition, the effluent stream is required to remove the formed dissolved SO_4^{2-} from the process solution. Whether the required effluent stream is based on discharge of produced SO_4^{2-} or on sulfur concentration in the thickened effluent stream strongly depends on the sulfur settling (box Figure 2). Assuming process conditions for a typical industrial BD facility (Table 1), the effluent stream will only be based on SO_4^{2-} discharge when the concentration of sulfur in the thickened effluent stream is higher than ~65 g L^{-1} (Figure 3). Below this concentration, the required effluent stream is solely defined by the sulfur concentration in the thickened effluent stream. For example, if the sulfur is poorly settleable and the concentration can only reach 20 g L^{-1}, the required effluent stream increases three-fold. This clearly illustrates that well settleable sulfur has a strong advantage over poorly settleable sulfur for process operation.

Table 1. Process conditions for a typical BD facility.

Process Condition	Value
Sulfur selectivity	85% [a]
Sulfate selectivity	15% [a]
Sulfate concentration	0.35 M [b]
Carbonate alkalinity	0.3 M [b]
Sodium concentration	1 M [b]
H_2S load	100 kg S day^{-1} [c]

[a] See Reference [7], [b] Values based on data collected in this study (Table A2 in Appendix A), [c] See Reference [24].

While it is known from industrial practice that sulfur particle properties differ between various facilities, the nature of these differences is still poorly understood. Understanding the sulfur particles' properties will provide information on how to control these properties. Therefore, we collected process solution samples from the bioreactor section from various industrial gas BD facilities in order to investigate the properties of the produced sulfur particles. Advantages of sampling industrial facilities

are (i) unlimited sample size, (ii) continuous operation, and (iii) representativeness of industrially produced sulfur. The sulfur particles in these samples were analyzed with respect to variation in morphology, size, composition, and settling behavior. Moreover, the relation between settleability, solids concentration, and particle size were investigated.

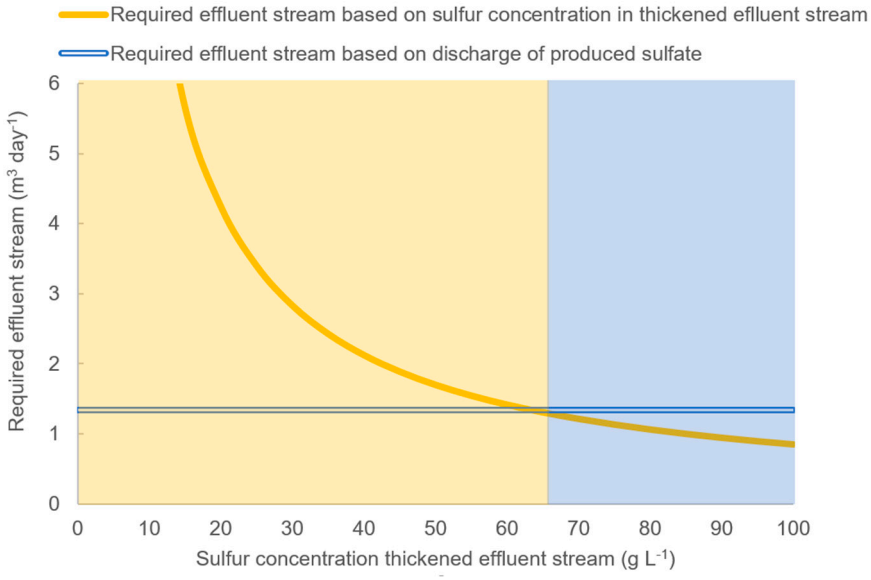

Figure 3. The relationship between sulfur concentration in the thickened effluent stream and the required effluent stream of a typical industrial BD facility. Only if the sulfur concentration in the thickened effluent stream is above 65 g L^{-1}, the required effluent stream will be based on discharge of produced sulfate (blue area, right). Below this "break-even point", the required effluent stream is solely dependent on sulfur concentration in the thickened effluent stream (yellow area, left).

2. Materials and Methods

2.1. Industrial Biological Biogas Desulfurization Facilities

Five industrial biological biogas desulfurization facilities in the Netherlands were sampled from the bioreactor section of the process: three facilities treating biogas from a paper mill, one facility treating biogas from a landfill, and one facility treating biogas from a cadaver disposal industry. Hereafter they are referred to as Paper mill 1–3, Landfill, and Cadaver. The bioreactor is a well-mixed, aerated tank. Liquid from the bioreactor was continuously pumped with a high flow rate over a bypass, from which a sample was taken.

2.2. Sampling Method

Prior to sample collection, the sampling point was flushed to remove any dried sulfur and as such to obtain a representative sample. The freshly harvested samples of 1 L each, were kept in glass Schott bottles and transported on ice, keeping the temperature at 2–3 °C. After transport, the samples were stored at 4 °C. At the time of sample collection, on-site measurements of the online-monitored operational data were obtained: temperature, pH, oxidation-reduction potential (ORP), and ORP set point for air dosing control. In addition, the presence of dissolved sulfide was tested directly after sampling on site with lead(II)acetate trihydrate paper (Aqualytic H_2S Test Paper 418701).

2.3. Chemical Analysis of Reactor Samples

Carbonate alkalinity was measured with a potentiometric titration (0.1 M HCl to pH 4.3, Titralab AT1000, Hach Lange, Germany). Concentrations of sulfate and thiosulfate were determined by ion chromatography (Dionex ICS 2100) with a Thermo Fisher Scientific IonPac AG17 Guard (Thermo

Fisher Scientific, Waltham, MA, USA) 4 × 50 mm and Thermo Fisher Scientific IonPac AS17 (Thermo Fisher Scientific) analytical 4 × 250 mm column at 30 °C and a flowrate of 1.0 mL min^{-1}. The injection volume was 10 µL. Data analysis was performed with Chromeleon™ 6.8 (Thermo Fisher Scientific). The bacteria concentration was measured as in [26]. Presence of biologically produced sulfur did not affect the results [7]. The sulfur concentration was determined by Standard Methods 2540D in triplicate [27]. Instead of the standard filter for this method, a glass microfiber filter with pore size 0.7 µm was used (Whatman, type GF/F). It is known that α-sulfur reacts to the β-polymorph at 95.2 °C. Thus, to avoid the reaction of sulfur to a different polymorph, the samples were dried overnight at 52 °C instead of 105 °C. pH offline was measured with a PHM 210 Standard pH meter (Radiometer Analytical SAS, Lyon, France). Conductivity was measured with an HQ440d multi-conductivity meter (Hach, Loveland, CO, USA).

2.4. Particle Analysis

The settleability of the sulfur particles was assessed with a settling column as described by Janssen et al. with a volume of 500 mL [28]. In addition, settling behavior under elevated 725× *g* was studied with a multi sample analytical centrifuge (LUMiSizer® 6112-70, L.U.M. GmbH, Berlin, Germany). Samples were transferred to polyamide/polycarbonate cells and the sedimentation speed was calculated from the transmission profiles (λ = 865 nm, sample cell [3] LUM 2 mm, PA/PC, Rect. Synthetic Cell (110-134xx/110-131xx), interval of 1–2 s. The samples were diluted with buffer (0.066 mol L^{-1} Na_2CO_3 and 0.874 mol L^{-1} $NaHCO_3$ in demi water) so that the final sulfur concentration equaled 1.5 mg g^{-1}. A carbonate buffer solution was used to maintain a similar conductivity and pH to the original samples as to eliminate the possible effects of changing those to parameters on the particle properties. Finally, in a separate experiment, 100 mL of the sample was left to settle for 2 h. Pictures were taken at t = 0 h and t = 2 h. The top layer of the sample was removed and analyzed for particle size distribution (PSD) and morphology with light microscopy. The bottom layer was also analyzed for PSD and morphology with light microscopy. The PSD was determined with a SALD-2300 Particle Size Analyzer (Shimadzu, Kyoto, Japan). The PSD was calculated from the data according to a combination of Fraunhofer diffraction theory and Mie scattering theory in which the refractive index of sulfur (α-S_8) was used (2.0) [29]. In addition, the PSD of the homogenous, original sample was measured. Particle morphology was studied by light microscopy with a Nikon Eclipse E400 (1000x magnification, Nikon, Tokyo, Japan) and the pictures taken and processed with Image Focus Alpha software (version 20-10-2018,, Euromex Microscopen BV, Arnhem, the Netherlands). In addition, particle morphology was studied with scanning electron microscopy. Samples were washed once with demi water to remove salts and dried overnight at room temperature. Subsequently, they were mounted on SEM stubs by carbon adhesive tabs (Electron Microscopy Sciences, Hatfield, PA, USA) and coated with 12 nm of Tungsten (Leica MED 020, Technical Applications & Microscopy Supplies, Schwerzenbach, Switzerland). Samples were analyzed at 2 kV, 6 pA, in a field emission scanning electron microscope (Magellan 400, FEI, Eindhoven, the Netherlands). Particle composition was studied by X-ray diffraction (XRD) with a Bruker D8 Advance equipped with Cu radiation (1600 W, Bruker, Billerica, MA, USA). The sample preparation was identical to the sample preparation for SEM. The samples were transferred to a zero-background Si wafer for XRD data collection. A Lynxeye XE-T detector (Bruker) was used with a position sensitive detection window set at 2.91°. The sample was spun at a speed of 5.0 rpm to ensure statistically optimal results. The scanning range was 10° to 60° 2θ and the step size was 0.015° with a step time of 0.5 s. Phase identification and quantification was done with Diffrac.EVA (version 4.2.1, Bruker) and the patterns were matched using the Crystallography Open Database (REV173445 2016.01.04). Zeta potential was measured with Nano Zetasizer (Malvern Panalytical, Malvern, UK). Prior to analysis the samples were dialyzed overnight to achieve a conductivity < 1 mS cm^{-1} to prevent electrode polarization during zeta potential measurement.

2.5. Error Calculation

Error values were determined by taking the difference between, respectively, the maximum value and the average (max-av), and the minimum value and the average (av-min) for triplicate measurements. In case of duplicates, the difference between the average and one of the values was used as error value. In case of single measurement, no error value is indicated.

3. Results and Discussion

3.1. Sulfur Particle Morphology and Size

The particles formed in the five industrial facilities were assessed on a number of properties. The particle morphology was distinctively different as seen with light microscopy in the original reactor fluid and with scanning electron microscopy (SEM) in the dried sample. (Figure 4). In the light microscopy pictures, the sulfur particles appear as white, translucent objects in the foreground. The black dots and stripes in the background are the HA-SOB. In the SEM pictures, the HA-SOB and salts are removed by a washing step, so only the sulfur particles are visible. With SEM it can be seen that the majority of the sulfur particles have a bipyramidal shape and their sizes range from 1 to 20 µm. The bipyramidal shape is typical for orthorhombic sulfur [30,31]. In addition, aggregates of sulfur particles are visible, ranging from small (5 µm) to larger aggregates (20 µm). This is especially visible in the light microscopy pictures.

Individual bipyramids are found in the samples of all paper mills. Paper mill 1 contains the largest individual bipyramidal particles of around 20 µm (Figure 4a) compared to the other paper mill samples. Paper mill 2 and Paper mill 3 show a combination of smaller, individual particles and aggregates (Figure 4g,i). In addition to the bipyramids, all samples contain small (<2 µm) globular structures, which are best visible in the sample of Paper mill 3 (Figure 4i). Such microbiologically formed sulfur globules were reported in earlier studies [28,32].

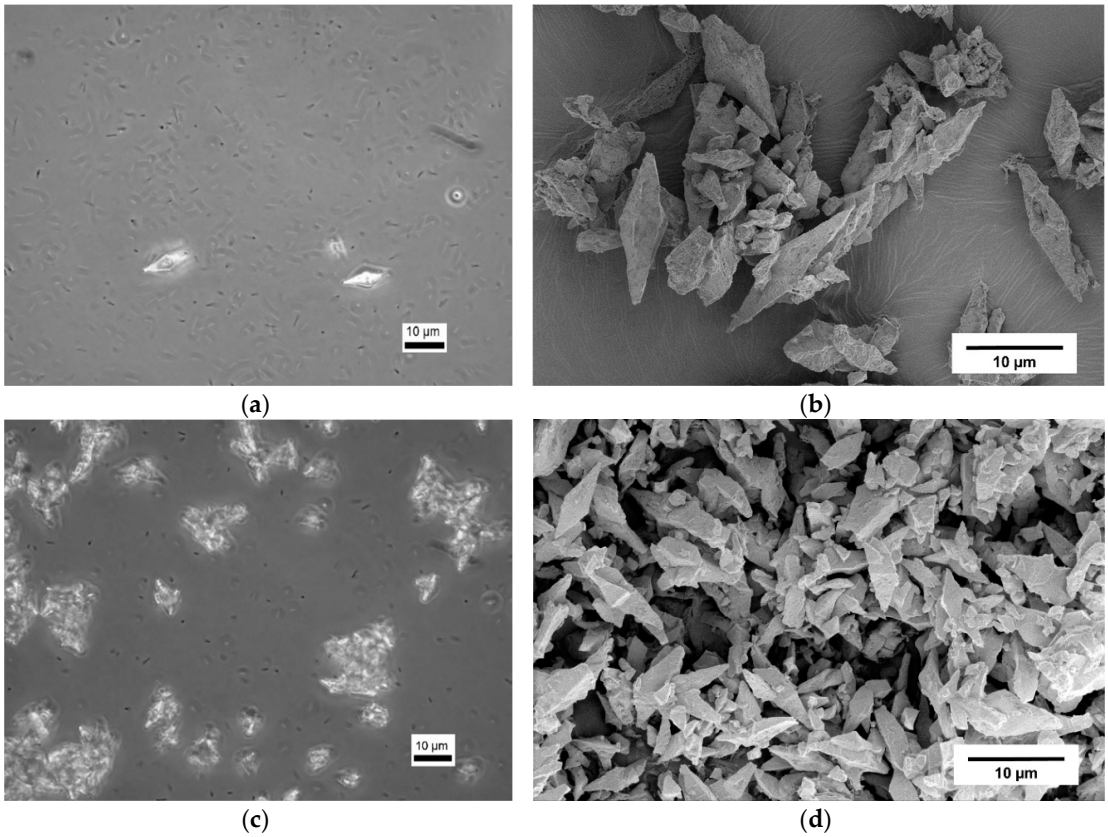

Figure 4. *Cont.*

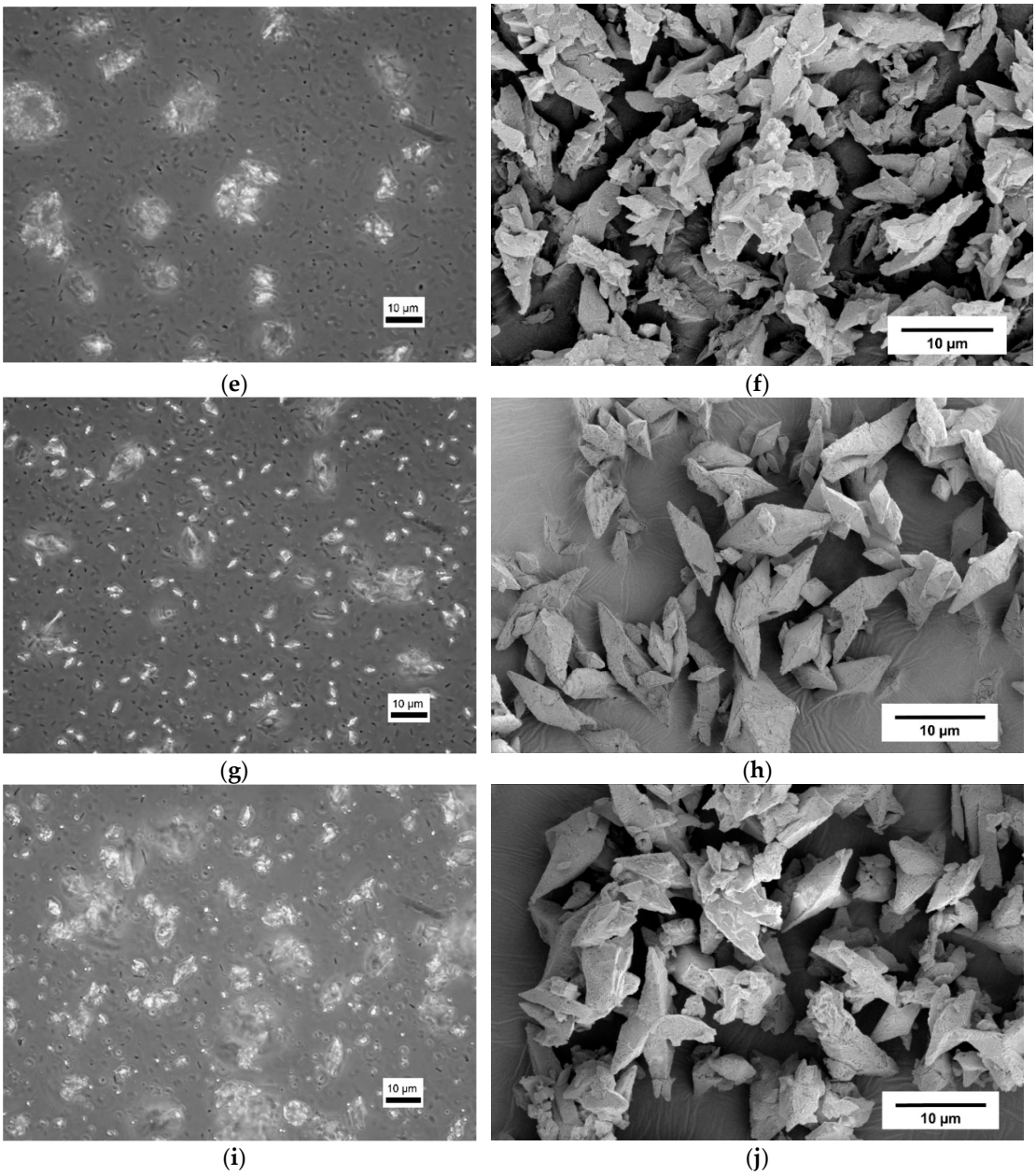

Figure 4. Light microscopy (**a**,**c**,**e**,**g**,**i**) and scanning electron microscopy (**b**,**d**,**f**,**h**,**j**) pictures of samples. From top to bottom: Paper mill 1 (**a**,**b**), Landfill (**c**,**d**), Cadaver (**e**,**f**), Paper mill 2 (**g**,**h**) and Paper mill 3 (**I**,**j**). The samples are presented from lowest to highest sulfur concentration. The sulfur concentrations of Paper mill 1, Land fill, Cadaver, Paper mill 2, and Paper mill 3 are 1.5, 11.1, 14.5, 16.9, and 29.4 mg g^{-1}, respectively.

In contrast to Paper mills 1–3, the particles from Landfill and Cadaver are more aggregated and do not contain single particles (Figure 4c,e). Aggregation is also observed in the SEM pictures. Bipyramids are visible, but they are interspersed with smaller particles that either adhere to the larger particles or are intergrown with them. It is possible that individual particles and aggregates are cemented together with formed sulfur, making them agglomerates [33]. On the SEM picture of Paper mill 1, aggregations are also visible. These aggregations are not visible in the light microscopy pictures, possibly due to the low sulfur concentration. However, they are visible in the concentrated sulfur slurry after sedimentation (Figure A1 in Appendix A).

To quantify the particle size, the particle size distribution (PSD) of the samples was measured with laser diffraction. In Figure 5, the full PSDs are shown for the volumetric- and numeric-based distribution. In a volumetric based distribution, larger particles have a heavier weight as, due to their size, they often comprise a larger percentage of the total solid volume. In a numeric-based distribution, each particle has an equal weight, independent of the particle size. For the purpose of solids separation, it is most interesting to interpret a volumetric-based PSD, as the interest lies in separating as much volume as possible. However, to reveal the presence of small particles, the numeric-based distribution is most suitable. Thus, both are discussed here. When reporting PSD, three values are commonly used: the D10, D50, and D90. They indicate the cut-off values for 10%, 50%, or 90% of the particles with a diameter less than the given diameter. "v" in Dv50 stands for "volumetric". The D10 and D90 values are reported in Appendix A (Table A1).

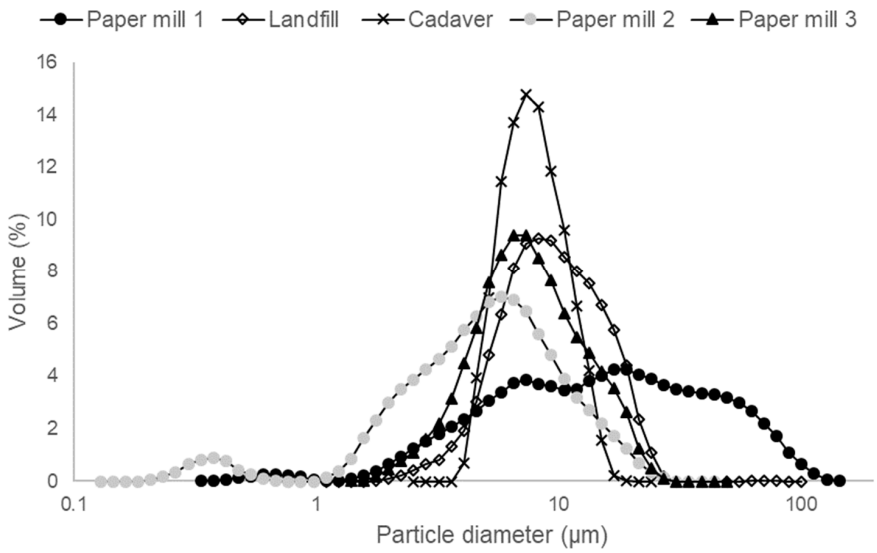

(**a**)

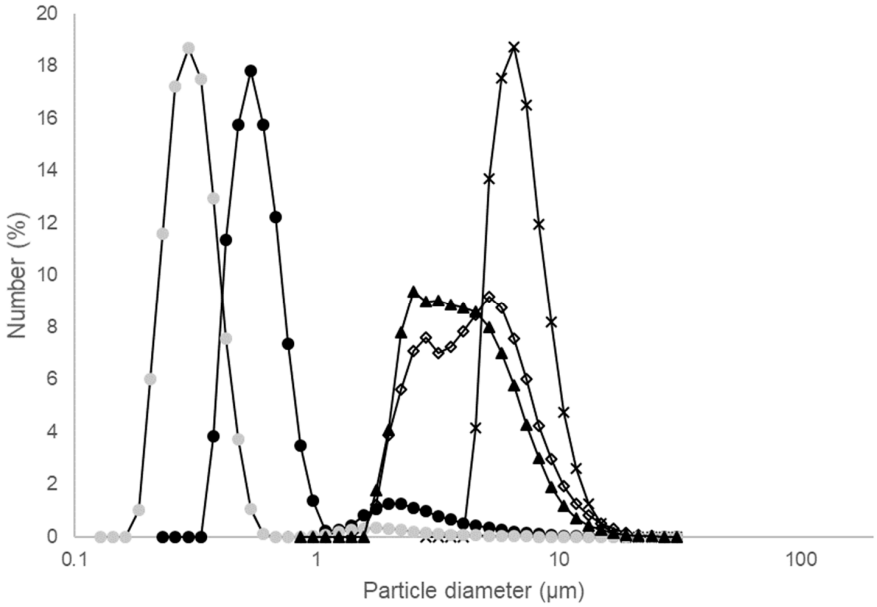

(**b**)

Figure 5. Volumetric (**a**) and numeric (**b**) based particle size distribution of Paper mill 1 (●); Landfill (◊); Cadaver (×); Paper mill 2 (●); Paper mill 3 (▲). Average maximum error is 0.21% (for volumetric) and 0.51% (for numeric).

Among the samples from the industrial facilities, Paper mill 1 contains the largest particles (D_V50 = 16.2 μm). In contrast, Paper mill 2 has the largest number of small particles (D_V50 = 5.5 μm). Landfill, Cadaver, and Paper mill 3 show similar morphology (aggregated particles) and this also shows in the Dv50s, which are similar and equal to 9.8, 9.2, and 7.8 μm, respectively. However, the PSD patterns differ in shape. Cadaver has the most monodisperse particles (of similar size, deduced from the sharp, slim peak), which can also be seen in the light microscopy picture. The aggregates visible in that picture are basically the same size (Figure 4e). The aggregates of Landfill are more polydisperse (of varying size, deduced from the broad peak), which is also visible in the light microscopy picture (Figure 4c). Paper mill 3 also shows a broad peak (polydisperse sample) but has a smaller Dv50 caused by the higher number of smaller particles. Cadaver, Landfill, and Paper Mill 3 clearly have larger particles (7.2, 4.7, and 3.6 μm) than Paper Mill 1 and 2 with Dn50 ("n" stands for numeric) of 0.6 and 0.3 μm, respectively (Figure 5b).

Although laser diffraction is generally recognized as one of the most reliable techniques for particle size analysis, the technique has some constraints, such as the assumption of particles being spherical. However, despite this constraint, the data from the laser diffraction is in good agreement with the particle size observed with microscopy.

3.2. Particle Settling

We performed three different settling tests on the samples. Settling is a complex process and quantification requires multiple validations, especially for small particles like the ones found in this study. An initial analysis of the samples' sedimentation behavior and rate involved a two-hour sedimentation test in 100 mL glass bottles. Pictures of the bottles with the samples were taken before and after the test (Appendix A Figure A2 before, Figure 6 after). For all samples, a distinct layer of sedimented sulfur could be observed, except for Paper mill 2 (green arrows). From Stokes' Law it was calculated that particles smaller than ~8 μm cannot settle 6 cm (length of the glass bottle) within the two-hour period, which explains the turbidity of Paper mill 2 and 3 as their Dv50 were lower than 8 μm.

It was observed that all particles from the top layers of the bottles (i.e., the non-sedimented fraction) had a Dv50 of around 2 μm (Figure 7). From the volume-based distribution for original, homogeneous sample (Figure 5), the volume fraction of non-sedimented sulfur was calculated. For Paper mill 2, this was the highest and equal to 2.7% of the total sulfur volume, representing 13.6% of the total sulfur particle number. The large amount of small, unsettling particles with a Dn50 of 0.3 μm and high surface to volume ratio in the Paper mill 2 sample will likely lead to operational interruption and increased influent and effluent volume as described in Figure 2 in the introduction. In comparison, for the other samples, the volume fractions that did not settle were the following: Paper mill 1 (1.0%), Landfill (0.8%), Cadaver (0.2%), and Paper mill 3 (0.7%). The non-sedimented fractions as calculated above are probably underestimated, because samples were taken only from the top 3 cm of the bottles, leaving out the bottom 3 cm. It means that in practice, the non-sedimented fractions are likely larger than reported here. The percentages indicate that in Paper mill 2, the small, unsettled particles take up a substantially larger part of the total solids than in, for example, Cadaver. Therefore, we conclude that the sulfur from Paper mill 2 had the lowest settleability of all five industrial facilities.

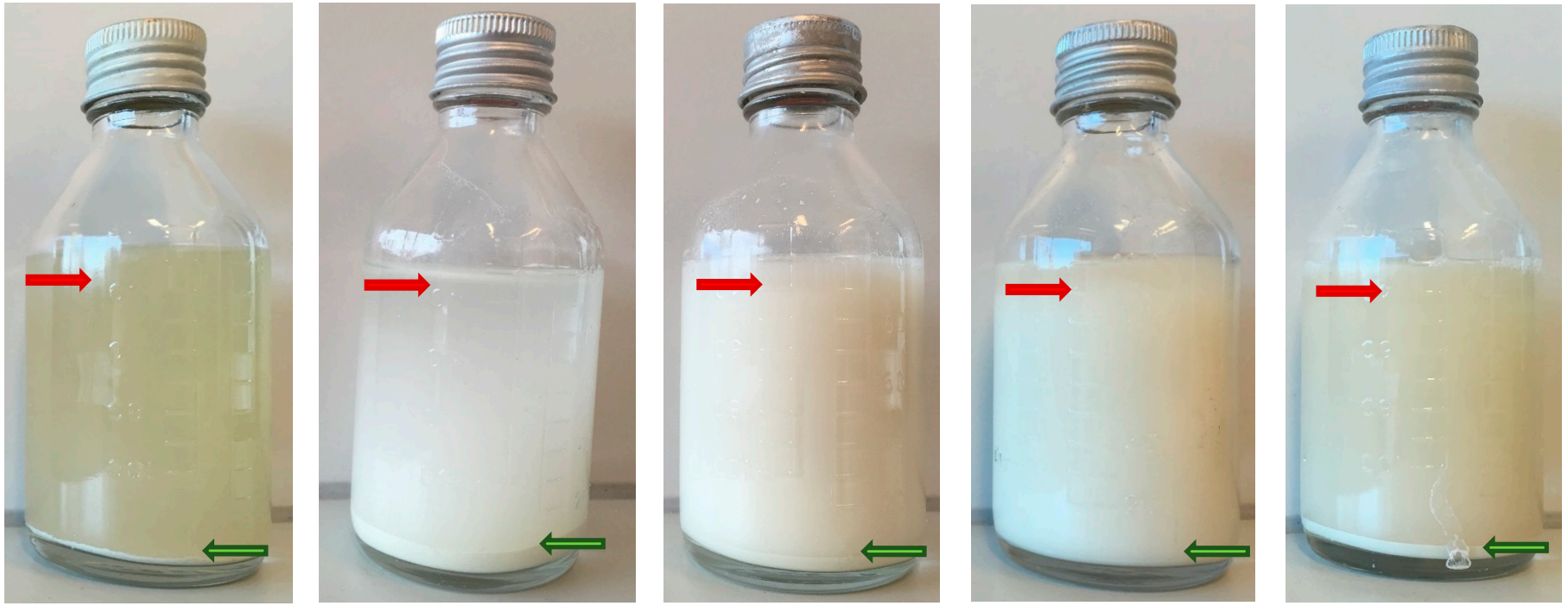

(**a**) (**b**) (**c**) (**d**) (**e**)

Figure 6. Bottles after 2 h of sedimentation. (**a**) Paper mill 1; (**b**) Landfill; (**c**) Cadaver; (**d**) Paper mill 2; (**e**) Paper mill 3. Red arrows indicate non-sedimented sulfur and green arrows sedimented sulfur.

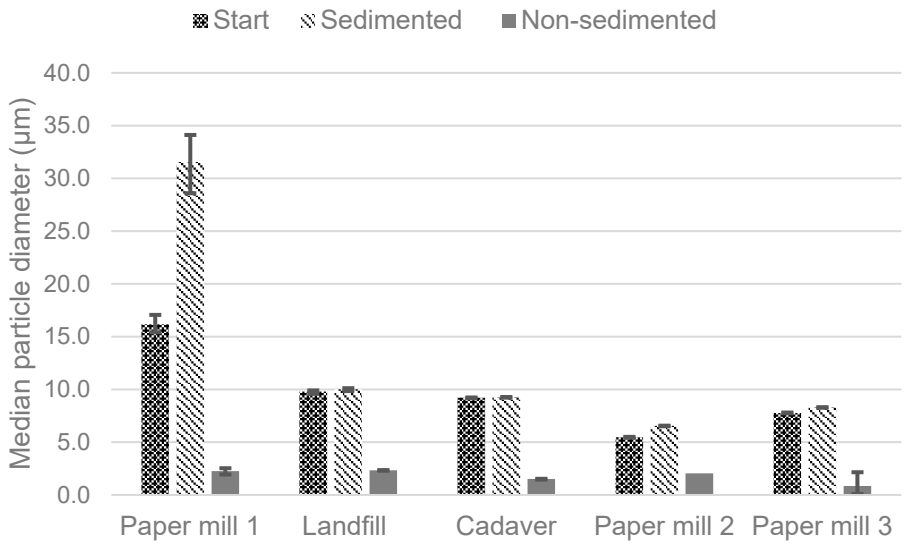

Figure 7. Median particle diameter (Dv50) of samples at the start of sedimentation, the sedimented layer, and the non-sedimented layer.

The sedimentation of the particles was also analyzed with a sedimentation column (Figure 8). Similar differences in settling were found as with the glass bottle sedimentation test. For Paper mill 1, 74.9% of the material settled within one hour, whereas for Paper mill 3 this was only 54.8%. The percentage of the sample settled at one hour for the other facilities was the following: Landfill (72.8%), Cadaver (66.2%), and Paper mill 2 (65.0%). In this test, Paper mill 3 showed the poorest settleability. However, the very high sulfur concentration (29.4 mg g^{-1}) could have led to hindered settling. After that, Paper mill 2 had the poorest settleability, similar to the bottle test.

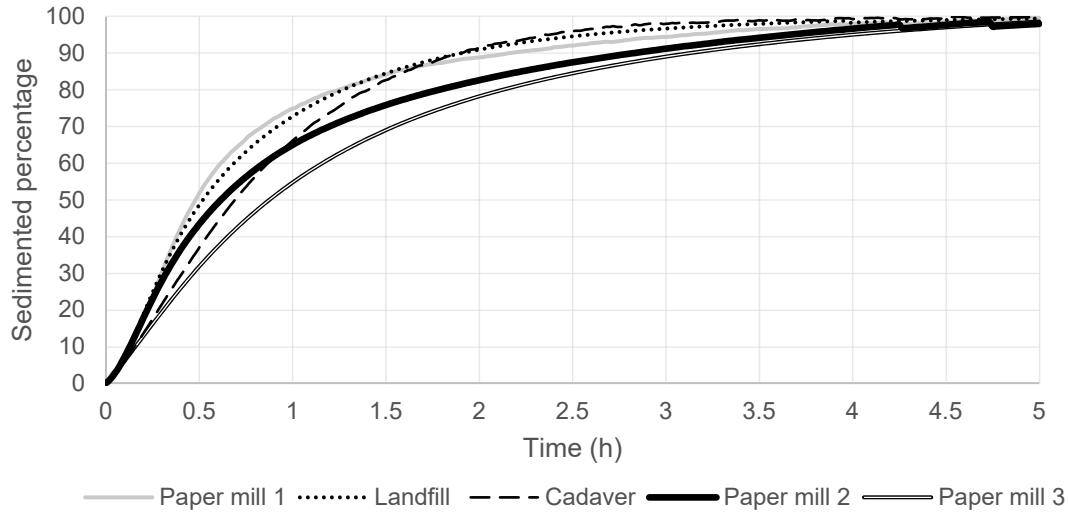

Figure 8. Sedimentation capacity of the sulfur particles measured with a sedimentation column.

Finally, the sedimentation velocity was also measured with an analytical ultracentrifuge at 725× *g*. Clear differences between the samples were found. For example, Cadaver had a median sedimentation velocity of 3.3 mm s^{-1}, whereas Paper mill 2 had a sedimentation velocity of 1.7 mm s^{-1}. The sedimentation velocities are compared with the sulfur concentration in Figure 9. A slight trend can be observed: a higher sedimentation velocity was found in samples with a relatively lower sulfur concentration (Paper mill 1, Land fill, and Cadaver), compared to a lower sedimentation velocity found in samples with a relatively higher sulfur concentration (Paper mill 2 and Paper mill 3). These two samples also have the smallest median particle sizes (Dv50 = 5.5 µm and Dv50 = 7.8 µm, respectively).

The higher sedimentation velocity of Paper mill 3 could have been caused by the larger particles in the sample. The data from Figure 9 confirms that in industrial BD reactors where the sulfur does not settle, it is likely that the particles will accumulate, leading to a higher sulfur solids concentration.

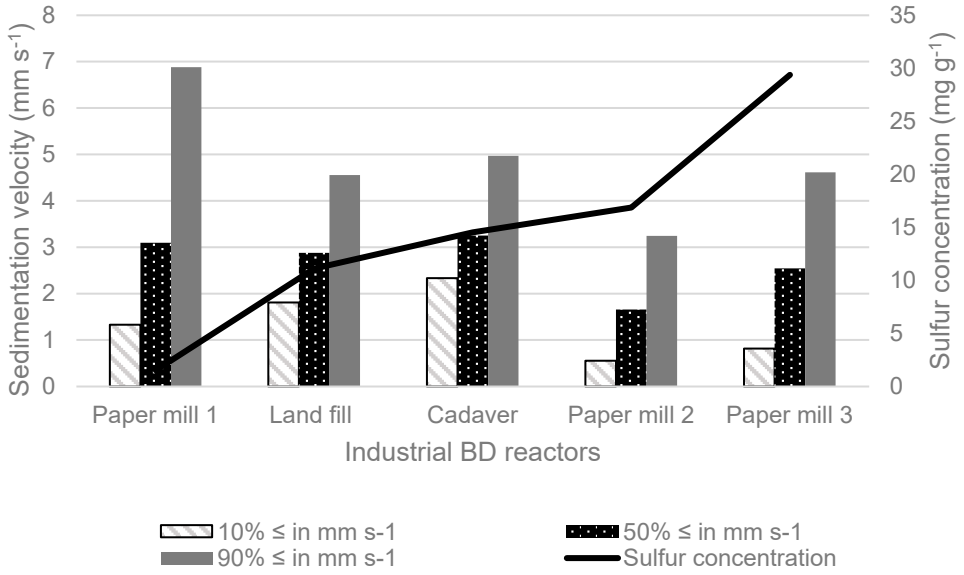

Figure 9. Sedimentation velocity at 725× *g* as compared to sulfur concentration. A light trend shows that samples with high sulfur concentration have lower sedimentation velocity.

3.3. Possible Explanations for Differences in Sulfur Particle Properties

We found significant differences in the particle morphology, size, and settling behavior of sulfur particles originating from a number of full-scale BD facilities. For example, sulfur particles formed in BD facility Paper mill 1 are the largest and showed the best settling properties. The aggregates found in Land fill, Cadaver, and Paper mill 3 also settled well. While the aggregates appeared the largest in the PSD, the SEM pictures indicated that those aggregates consist of a cluster of smaller particles (Figure 4). The particles in the aggregates were smaller compared to the individual particles from Paper mill 2. To understand how these differences emerged in the full-scale BD facilities, it is important to explain how the sulfur particles are produced and how their crystallization works.

Crystallization is a highly complex process in which many parameters influence the growth kinetics. As a result, the properties of the formed product (elemental sulfur) vary with changing process conditions. One crucial parameter in formation and growth of crystals is the supersaturation of the solution in which the crystals are formed [34]. Supersaturation takes place if the concentration of product in the solution is larger than the maximum solubility. At supersaturation, nucleation takes place. Nucleation occurs if the Gibbs energy of formation with a certain particle radius defined by the thermodynamic driving force from the bulk solution and the surface energy that needs to be overcome is positive. Whereas under high supersaturation nucleation is induced, low supersaturation stimulates crystal growth (also called the metastable zone). Known parameters that can affect crystallization are (i) chemical solution composition, (ii) temperature, (iii) rate of substrate formation for crystal growth and its solubility, and (iv) particle interactions, such as turbulence, steric hindrance, and charge repulsion.

Yet, for sulfur, nucleation is expected to occur already at very low concentration, due to the very low solubility of orthorhombic S_8 (the most encountered polymorph of sulfur in nature) in water (5 μg L^{-1}) [35]. Urakaev et al. modelled the formation of amorphous sulfur nuclei and predicted that the most probable size of a sulfur nucleus is 2.6 nm [36], which is much smaller than we could have observed with microscopy in our samples. We did observe and measure (globular, amorphous) submicron particles, but these are expected to mature during their retention time in the BD bioreactor. All samples (after drying) were confirmed to be orthorhombic α-S_8 with X-ray diffraction (Appendix A Figure A3). For crystallization this means that there was no difference in crystal structure between the

samples. In addition, sulfur is a strongly hydrophobic, molecular crystal, which makes crystallization very different from, for example, an ionic crystal such as NaCl. Sulfur crystallization can best be described as a type of "precipitation" or "reactive crystallization". This fast process results in rapid solid formation of extremely small crystals [37]. These can then form agglomerates by cementation by the build-up of a crystalline bridge and usually will prevail in a supersaturated solution [38]. In addition, agglomeration lowers the surface energy [39]. The reactive crystallization process could explain the aggregate/agglomerate formation in the BD facilities. Contrary to the samples with aggregates, the sample of Paper mill 2 contained many clearly defined, separate idiomorphic crystals of which the smaller ones did not settle. Presumably, these bipyramidal crystals were grown in the metastable zone, where the concentration of molecules is above maximum solubility, but not high enough to form new nuclei. Hence, in the metastable zone, crystal growth is promoted.

Whether the crystallization conditions in a BD facility are more favorable for nucleation or growth can be affected by the operational conditions. For examples, the specific sulfide oxidation rate that controls how fast sulfur is formed depends on the type and number of bacteria present, which in turn is affected by operation conditions. Values for operational and chemical parameters of the five industrial BD facilities can be found in Table A2. Differences are found in chemical composition, such as in conductivity (ranging from 39.2–81.5 mS cm^{-1}) and bacteria concentration (ranging from 10–51 mg N L^{-1}). The differences in process conditions can be explained by, for example, the differences in operation strategy, design of the process and feed gas composition, and flow rate. However, since in this study only five industrial facilities were sampled, no statistical tests can be performed on the correlation of operational conditions with particle properties. To obtain more insight into the effect of the operational conditions in the BD process on sulfur particle properties, reactor experiments have to be performed in which factors such as presence of impurities, sulfur chemistry kinetics, sulfide oxidation rate, and sulfide loading rate are studied. These factors are expected to have a strong influence on the driving force from the bulk and thereby on sulfur particle growth. Insight into those factors is crucial to explain the sulfur crystallization and aggregation in the biological desulfurization process of gas for the optimization of sulfur settling, enhancing process operability.

4. Conclusions

In this paper, we investigated the properties of sulfur formed in five industrial BD facilities. Distinct differences in sulfur particle size, shape, sedimentation rate, and behavior were demonstrated. In some facilities, the sulfur was present as aggregates, whereas in other facilities the sulfur particles were present as individual bipyramidal crystals. The formation of aggregates or growth of larger crystals is essential to efficiently recover the sulfur particles from the process solution, as well as to prevent the formation of small particles that can hinder process operation. The differences in sulfur particle properties are very likely caused by variations in operational conditions. The operational conditions affect sulfur supersaturation, and thereby the crystallization of the sulfur particles. Therefore, for future research, it is necessary to investigate what are the main operational factors defining sulfur crystallization and aggregation in the biological desulfurization process to better control the process.

Author Contributions: Conceptualization, C.J.N.B.; formal analysis, A.R.M., R.D.v.d.W., J.B.M.K. and C.J.N.B.; funding acquisition, J.B.M.K.; investigation, A.R.M.; methodology, A.R.M.; Supervision, R.D.v.d.W., J.B.M.K. and C.J.N.B.; visualization, A.R.M.; writing—original draft, A.R.M.; writing—review and editing, R.D.v.d.W., J.B.M.K. and C.J.N.B. All authors have read and agree to the published version of the manuscript.

Funding: This research was funded by Paqell B.V.

Acknowledgments: We thank Klaus Mannweiler of GEA Westfalia Separator Group GmbH for the LUMiSizer® analyses, the sulfur thesis ring for their fruitful comments, and Lourens van Langeveld for laying the foundation for the some of the analyses in this paper. We thank Marcel Giesbers from the Wageningen Electron Microscopy Centre for taking the SEM pictures.

Conflicts of Interest: A.R.M. and J.B.M.K. are on secondment at Wageningen University & Research. They are obligated to follow the Netherlands Code of Conduct for Research Integrity. Wageningen University & Research holds responsibility for this.

Appendix A

Table A1. Particle properties of samples harvested from the five industrial facilities.

Parameter	Paper Mill 1	Land Fill	Cadaver	Paper Mill 2	Paper Mill 3
TSS (mg g^{-1}) [a]	1.5	11.1	14.5	16.9	29.4
Settled after 1 h (%) [b]	74.9	72.8	66.2	65.0	54.8
Settled after 2 h (%) [c]	88.9	91.0	91.5	82.7	78.3
Sedimentation Velocity (Under Elevated g)					
10% ≤ (μm s^{-1})	1330 ± 16	1808 ± 52	2333 ± 92	554 ± 23	814 ± 127
50% ≤ (μm s^{-1})	3097 ± 29	2877 ± 22	3251 ± 67	1657 ± 83	2543 ± 6
90% ≤ (μm s^{-1})	6880 ± 1369	4554 ± 411	4971 ± 908	3244 ± 322	4614 ± 356
Particle Size [d,e]					
D_v10% (μm)	4.0	5.3	6.3	2.0	4.1
D_v50% (μm)	16.2	9.8	9.2	5.5	7.8
D_v90% (μm)	59.3	18.5	14.1	12.9	16.0
$Modal_v$ (μm)	19.0	9.3	9.3	5.8	7.3
D_n10% (μm)	0.4	2.5	5.3	0.2	2.1
D_n50% (μm)	0.6	4.7	7.2	0.3	3.6
D_n90% (μm)	1.6	8.9	10.5	0.5	7.0
$Modal_n$ (μm)	0.6	5.6	7.1	0.3	2.8
Zeta potential (mV) [f]	−21.2	−21.0	−21.9	−18.5	−23.7

[a] ± <0.1 mg g^{-1}; [b] ± <4.7%; [c] ± <3.0%; [d] Volume based distribution error of ± <0.2 μm except for paper mill 1 with D_v50% ± <0.9 μm and D_v90% ± <3.6 μm; [e] Numeric based distribution error of ± <0.3 μm; [f] ± <0.9 mV.

Table A2. Values for operational and chemical parameters for two of the five studied BD facilities.

Parameter	Paper Mill 1	Land Fill	Cadaver	Paper Mill 2	Paper Mill 3
ORP set-point (mV vs. Ag/AgCl)	−370	−320	−350	−370	−380
ORP (mV vs. Ag/AgCl)	−393	−298	−347	−377	−35 [b]
pH online (-)	8.54	8.11	8.38	8.43	8.50
pH offline (-)	8.64	8.42	8.37	8.70	8.73
Temperature (°C)	39.2	31.1	34.5	36.9	34.4
Conductivity (mS cm^{-1})	61	39.2	81.5	45.9	64.2
[Na+] (M)	1.06	0.68	1.55	0.78	1.30
Alkalinity (M)	0.31	0.60	0.18	0.55	0.96
SO_4^{2-} concentration (g L^{-1})	36.2	3.9	50.7	9.7	15.6
$S_2O_3^{2-}$ concentration (g L^{-1})	<LOD [a]	<LOD	17.6	1.8	0.5
Biomass concentration (mg N L^{-1})	51	29	39	10	Missing
HS^- present	no	no	no	no	no

[a] Limit of detection (LOD) was 5 mg L^{-1}; [b] H_2S flow temporarily stopped during sampling moment explaining high oxidation-reduction potential (ORP).

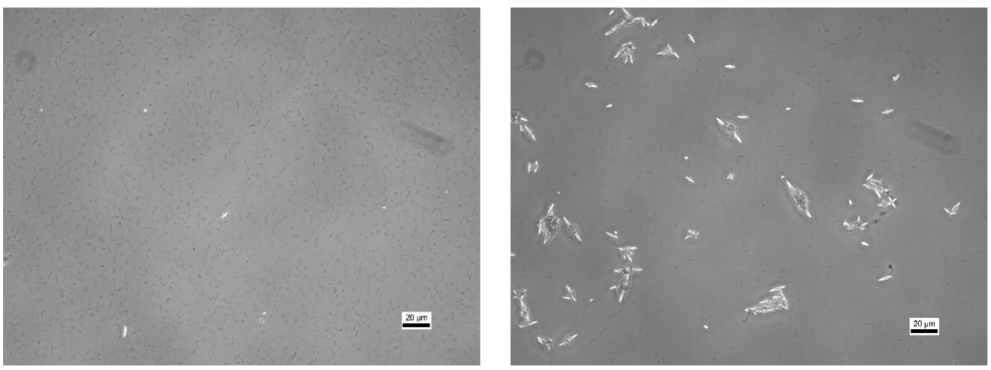

(**a**) (**b**)

Figure A1. *Cont.*

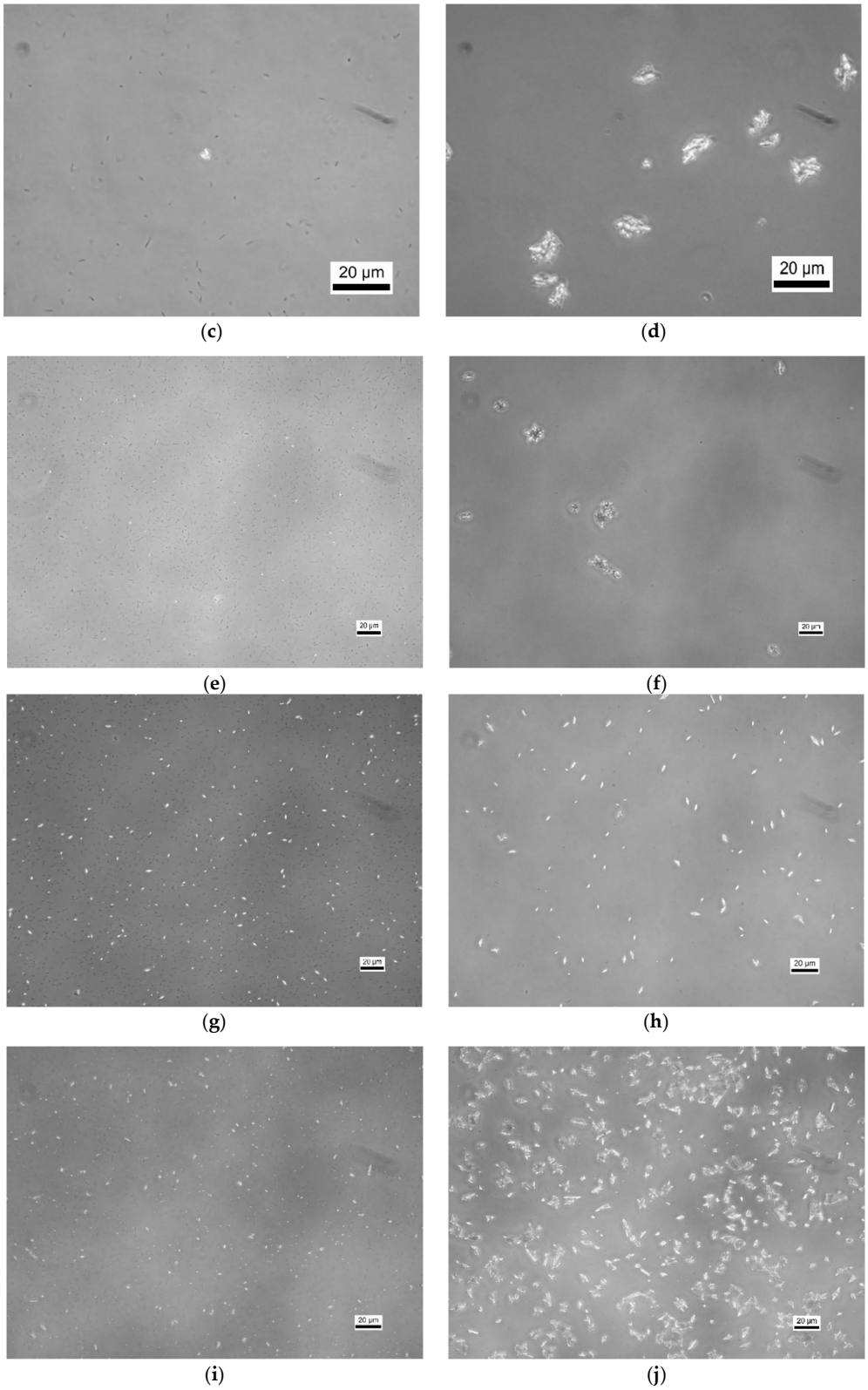

Figure A1. Light microscopy pictures of samples: top layer of the bottle (**a**,**c**,**e**,**g**,**i**) and bottom layer of the bottle (**b**,**d**,**f**,**h**,**j**) after 2 h of sedimentation. From top to bottom: Paper mill 1 (**a**,**b**), Landfill (**c**,**d**), Cadaver (**e**,**f**), Paper mill 2 (**g**,**h**), and Paper mill 3 (**i**,**j**).

(a) (b) (c) (d) (e)

Figure A2. Bottles before 2 h of sedimentation. (**a**) Paper mill 1; (**b**) Landfill; (**c**) Cadaver; (**d**) Paper mill 2; (**e**) Paper mill 3.

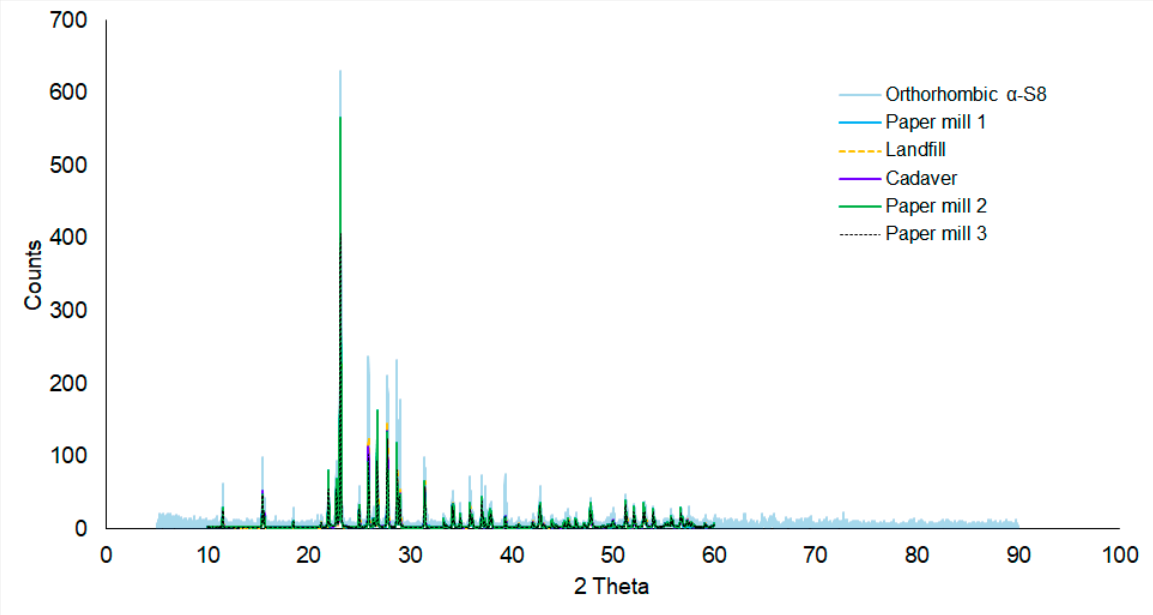

Figure A3. Diffraction patterns for the five sulfur samples from the different industrial BD facilities. All five samples show an identical diffraction pattern matching with the pattern for orthorhombic α-S_8 [40].

References

1. Chynoweth, D.P.; Owens, J.M.; Legrand, R. Renewable methane from anaerobic digestion of biomass. *Renew. Energy* **2000**, *22*, 1–8. [CrossRef]
2. Weiland, P. Biogas production: Current state and perspectives. *Appl. Microbiol. Biotechnol.* **2010**, *85*, 849–860. [CrossRef] [PubMed]
3. Holm-Nielsen, J.B.; Al Seadi, T.; Oleskowicz-Popiel, P. The future of anaerobic digestion and biogas utilization. *Bioresour. Technol.* **2009**, *100*, 5478–5484. [CrossRef] [PubMed]
4. Smith, S.J.; Van Aardenne, J.; Klimont, Z.; Andres, R.J.; Volke, A.; Delgado Arias, S. Anthropogenic sulfur dioxide emissions: 1850–2005. *Atmos. Chem. Phys.* **2011**, *11*, 1101–1116. [CrossRef]
5. Klimont, Z.; Smith, S.J.; Cofala, J. The last decade of global anthropogenic sulfur dioxide: 2000–2011 emissions. *Environ. Res. Lett.* **2013**, *8*, 014003. [CrossRef]
6. Cline, C.; Hoksberg, A.; Abry, R.; Janssen, A.J.H. Biological process for H_2S removal from gas streams the shell-paques/thiopaq^{TM} gas desulfurization process. In Proceedings of the Laurance Reid Gas Conditioning Conference, Norman, OK, USA, 23–26 February 2003.
7. Van Den Bosch, P.L.F.; Van Beusekom, O.C.; Buisman, C.J.N.; Janssen, A.J.H. Sulfide oxidation at halo-alkaline conditions in a fed-batch bioreactor. *Biotechnol. Bioeng.* **2007**, *97*, 1053–1063. [CrossRef]
8. Van Zessen, E.; Janssen, A.J.H.; De Keizer, A.; Heine, B.; Peace, J.; Abry, R. Application of THIOPAQ TM biosulphur in agriculture. In Proceedings of the Br. Sulphus Events 2004 Sulphur Conference, Barcelona, Spain, 24–27 October 2004; pp. 57–68.
9. Schils, R. *30 Vragen en Antwoorden Over Zwavel*; Alterra, Wageningen UR: Wageningen, The Netherlands, 2016.
10. Lim, J.; Pyun, J.; Char, K. Recent approaches for the direct use of elemental sulfur in the synthesis and processing of advanced materials. *Angew. Chem. Int. Ed.* **2015**, *54*, 3249–3258. [CrossRef]
11. Ucar, D.; Yilmaz, T.; Di Capua, F.; Esposito, G.; Sahinkaya, E. Comparison of biogenic and chemical sulfur as electron donors for autotrophic denitrification in sulfur-fed membrane bioreactor (SMBR). *Bioresour. Technol.* **2020**, *299*, 122574. [CrossRef]
12. Di Capua, F.; Ahoranta, S.H.; Papirio, S.; Lens, P.N.L.; Esposito, G. Impacts of sulfur source and temperature on sulfur-driven denitrification by pure and mixed cultures of Thiobacillus. *Process Biochem.* **2016**, *51*, 1576–1584. [CrossRef]

13. Seidel, H.; Wennrich, R.; Hoffmann, P.; Löser, C. Effect of different types of elemental sulfur on bioleaching of heavy metals from contaminated sediments. *Chemosphere* **2006**, *62*, 1444–1453. [CrossRef]
14. Zhu, T.T.; Cheng, H.Y.; Yang, L.H.; Su, S.G.; Wang, H.C.; Wang, S.S.; Wang, A.J. Coupled Sulfur and Iron(II) Carbonate-Driven Autotrophic Denitrification for Significantly Enhanced Nitrate Removal. *Environ. Sci. Technol.* **2019**, *53*, 1545–1554. [CrossRef]
15. Florentino, A.P.; Weijma, J.; Stams, A.J.M.; Sánchez-Andrea, I. Sulfur Reduction in Acid Rock Drainage Environments. *Environ. Sci. Technol.* **2015**, *49*, 11746–11755. [CrossRef]
16. Janssen, A.J.H.; Lens, P.N.L.; Stams, A.J.M.; Plugge, C.M.; Sorokin, D.Y.; Muyzer, G.; Dijkman, H.; Van Zessen, E.; Luimes, P.; Buisman, C.J.N. Application of bacteria involved in the biological sulfur cycle for paper mill effluent purification. *Sci. Total Environ.* **2009**, *407*, 1333–1343. [CrossRef]
17. Klok, J.B.; van Heeringen, G.; de Rink, R.; Wijnbelt, H.; Bowerbank, G. Techno-Economic Impact of the Next Generation Thiopaq O&G Process for Sulfur Removal. In Proceedings of the GPA-GCC, Muscat, Oman, 6–8 March 2018.
18. Klok, J.B.; van Heeringen, G.; De Rink, R.; Wijnbelt, H. Introducing the next generation of the THIOPAQ O&G process for biotechnological gas desulphurization: THIOPAQ-SQ. *Sulphur* **2017**, *18260*, 1–2.
19. Buisman, C.J.; Geraats, B.G.; Ijspeert, P.; Lettinga, G. Optimization of sulphur production in a biotechnological sulphide-removing reactor. *Biotechnol. Bioeng.* **1990**, *35*, 50–56. [CrossRef]
20. Janssen, A.J.H.; Lettinga, G.; Keizer, A. De Removal of hydrogen sulphide from wastewater and waste gases by biological conversion to elemental sulphur Colloidal and interfacial aspects of biologically produced sulphur particles. *Colloids Surf. A Physicochem. Eng. Asp.* **1999**, *151*, 389–397. [CrossRef]
21. Kleinjan, W.E.; De Keizer, A.; Janssen, A.J.H. Biologically produced sulfur. In *Topics in Current Chemistry*; Springer: Berlin/Heidelberg, Germany, 2003; pp. 167–188.
22. Klok, J.B.M.; Van Den Bosch, P.L.F.; Buisman, C.J.N.; Stams, A.J.M.; Keesman, K.J.; Janssen, A.J.H. Pathways of sulfide oxidation by haloalkaliphilic bacteria in limited-oxygen gas lift bioreactors. *Environ. Sci. Technol.* **2012**, *46*, 7581–7586. [CrossRef]
23. Roman, P.; Bijmans, M.F.M.; Janssen, A.J.H. Influence of methanethiol on biological sulphide oxidation in gas treatment system. *Environ. Technol. (UK)* **2016**, *37*, 1693–1703. [CrossRef]
24. Klok, J.B.M. (Paqell B.V., Utrecht, The Netherlands). Personal communication, 2016.
25. Kleinjan, W.E.; Marcelis, C.L.M.; De Keizer, A.; Janssen, A.J.H.; Stuart, M.A.C. Foam formation in a biotechnological process for the removal of hydrogen sulfide from gas streams. *Colloids Surf. A Physicochem. Eng. Asp.* **2006**, *275*, 36–44. [CrossRef]
26. De Rink, R.; Klok, J.B.M.; Van Heeringen, G.J.; Sorokin, D.Y.; Heijne, A.; Zeijlmaker, R.; Mos, Y.M.; De Wilde, V.; Keesman, K.J.; Buisman, C.J.N. Increasing the Selectivity for Sulfur Formation in Biological Gas Desulfurization. *Environ. Sci. Technol.* **2019**, *53*, 4519–4527. [CrossRef]
27. *American Public Health Assocation and American Water Works Association Standard Methods for the Examination of Water and Wastewater*; American Public Health Association: Washington, DC, USA, 1989.
28. Janssen, A.J.H.; De Keizer, A.; Van Aelst, A.; Fokkink, R.; Yangling, H.; Lettinga, G. Surface characteristics and aggregation of microbiologically produced sulphur particles in relation to the process conditions. *Colloids Surf. B Biointerfaces* **1996**, *6*, 115–129. [CrossRef]
29. Lide, D.R. *CRC Handbook of Chemistry and Physics*; Internet, V., Ed.; CRC Press: Boca Raton, FL, USA, 2005.
30. Betechtin, A.G. Schwefel-Gruppe. In *Lehrbuch der Speziellen Mineralogie*; VEB Deutscher Verlag für Grundstoffindustrie: Leipzig, Germany, 1977; pp. 158–161.
31. Fu, Y.; Manthiram, A. Orthorhombic Bipyramidal Sulfur Coated with Polypyrrole Nanolayers as a Cathode Material for Lithium—Sulfur Batteries. *J. Phys. Chem. C* **2012**, *116*, 8910–8915. [CrossRef]
32. Hanson, T.E.; Bonsu, E.; Tuerk, A.; Marnocha, C.L.; Powell, D.H.; Chan, C.S. Chlorobaculum tepidum growth on biogenic S(0) as the sole photosynthetic electron donor. *Environ. Microbiol.* **2016**, *18*, 2856–2867. [CrossRef]
33. Lewis, A.; Seckler, M.; Kramer, H.; van Rosmalen, G. 6.3 The agglomeration process. In *Industrial Crystallization Fundamental and Applications*; Cambridge University Press: Cambridge, UK, 2015; pp. 132–133.
34. Lewis, A.; Seckler, M.; Kramer, H.; van Rosmalen, G. 1.5 Supersaturation. In *Industrial Crystallization Fundamental and Applications*; Cambridge University Press: Cambridge, UK, 2015; pp. 14–15.
35. Boulègue, J. Solubility of Elemental Sulfur in Water at 298 KNo Title. *Phosphorus Sulfur Relat. Elem.* **1978**, *5*, 127–128. [CrossRef]

36. Urakaev, F.K.; Drebushchak, T.N.; Savintsev, Y.P.; Drebushchak, V.A. Mechanism and modelling of formation of amorphous sulfur nuclei. *Mendeleev Commun.* **2003**, *13*, 37–38. [CrossRef]
37. Lewis, A.; Seckler, M.; Kramer, H.; van Rosmalen, G. Precipitation and anti-solvent crystallization. In *Industrial Crystallization Fundamental and Applications*; Cambridge University Press: Cambridge, UK, 2015; pp. 234–260.
38. Lindenberg, C.; Vicum, L.; Mazzotti, M. L-Glutamic Acid Precipitation: Agglomeration Effects. *Cryst. Growth Des.* **2008**, *8*, 224–237. [CrossRef]
39. Lewis, A.; Seckler, M.; Kramer, H.; van Rosmalen, G. 4.2.1.1 Nucleus size. In *Industrial Crystallization Fundamentals and Applications*; Cambridge University Press: Cambridge, UK, 2015; p. 72. ISBN 978-1-107-05215-4.
40. Lafuente, B.; Downs, R.T.; Yang, H.; Stone, N. The power of databases: The RRUFF project. In *Highlights in Mineralogical Crystallography*; W. De Gruyter: Berlin, Germany, 2015; pp. 1–30.